Published in : Macromolecular Rapid Communications (2019), vol. 40, issue 1, pp. 1-6
doi.org/10.1002/marc.201800545
Status : Postprint (Author's version)

POLY(IONIC LIQUID)-DERIVED N-DOPED CARBONS WITH HIERARCHICAL POROSITY FOR LITHIUM- AND SODIUM-ION BATTERIES

Walid Alkarmo[1], Farid Ouhib[1], Abdelhafid Aqil[1], Jean-Michel Thomassin[1], Jiayin Yuan[2], Jiang Gong[3], Bénédicte Vertruyen[4], Christophe Detrembleur[1], and Christine Jérôme[1]

[1]*Centre for Education and Research on Macromolecules, CESAM Research Unit, University of Liege, Sart-Tilman B6a, 13 allée du 6 août, B-4000 Liège, Belgium*
E-mail: c.jerome@uliege.be
[2]*Department of Materials and Environmental Chemistry, Stockholm University, Svante Arrheniusvag 16C, 10691 Stockholm, Sweden*
E-mail: jiayin.yuan@mmk.su.se
[3]*Key Laboratory for Material Chemistry of Energy Conversion and Storage, Ministry of Education, School of Chemistry and Chemical Engineering, Huazhong University of Science and Technology, Wuhan 430074, China*
[4]*GREENMAT, CESAM Research Unit, University of Liège, Sart Tilman B6a, 4000 Liège, Belgium*

Abstract

The performance of lithium- and sodium-ion batteries relies notably on the accessibility to carbon electrodes of controllable porous structure and chemical composition. This work reports a facile synthesis of well-defined N-doped porous carbons (NPCs) using a poly(ionic liquid) (PIL) as precursor, and graphene oxide (GO)-stabilized poly(methyl methacrylate) (PMMA) nano particles as sacrificial template. The GO-stabilized PMMA nanoparticles are first prepared and then decorated by a thin PIL coating before carbonization. The resulting NPCs reach a satisfactory specific surface area of up to 561 m^2 g^{-1} and a hierarchically meso- and macroporous structure while keeping a nitrogen content of 2.6 wt%. Such NPCs deliver a high reversible charge/discharge capacity of 1013 mA h g^{-1} over 200 cycles at 0.4 A g^{-1} for lithium-ion batteries, and show a good capacity of 204 mA h g^{-1} over 100 cycles at 0.1 A g^{-1} for sodium-ion batteries.

Keywords

lithium-ion batteries, poly(ionic liquid), porous carbon, sodium-ion batteries

In the past decades, nitrogen-doped porous carbons (NPCs) have attracted wide interest due to their potential in catalysis,[1] membrane separation,[2] CO_2 capture,[3] and energy technologies such as batteries,[4] fuel cells,[5] and supercapacitors.[6] NPCs are particularly interesting for lithium-ion batteries (LIBs) and very recently also for sodium-ion batteries (SIBs).[7] The incorporation of N atoms favors some physical properties of NPCs by raising the overall electron density to enhance the electrochemical stability and charge mobility.[8] Furthermore, N dopant can carry surface functionality easily and a large number of defects to assist Li^+ or Na^+ insertion.[9,10] Meanwhile, pores in such a carbon matrix provide highways to Li^+ (or Na^+) diffusion and offer a large electrolyte–electrode interface for charge/ mass transfer, thus enhancing specific capacity and rate performance.[11] Last but not least, these pores act as an ion reservoir

Published in : Macromolecular Rapid Communications (2019), vol. 40, issue 1, pp. 1-6
doi.org/10.1002/marc.201800545
Status : Postprint (Author's version)

and provide space to buffer volume expansion during Li^+ or Na^+ insertion/extraction to improve cycling stability.[12]

In general, NPCs are produced by pyrolysis of N-containing compounds such as synthetic polymers,[13] organic salts,[14] fossil fuels,[15] and biomass.[16] In terms of synthetic polymers, such as phenolic resins,[17] their easy access and processing are the major factors to be considered. In addition, some monomers such as pyrrole[18] may require metal catalysts for poly merization, leading to concerns of metal contamination. Moreover, extents of doping and graphitization, which affect electric conductivity, are important and can affect which polymer precursors are chosen. For example, the inherent nature of "hard carbon" precursors such as furfuryl and alcohol sucrose gives low graphitization degree at temperatures below 1200 °C.[19] Numerous researchers in this field have confirmed that a broad range of properties of carbon materials depends on the chemical nature and morphology of the polymer precursors,[20–22] among which poly(ionic liquid)s (PILs) are an innovative class of carbon precursors.[23] In comparison to other polymers such as polyacrylonitrile, polypyrrole, and polydopamine, PILs possess several unique features. First, PILs present relatively high thermostability which leads to a high carbonization yield.[24] Second, they have diverse molecular structures carrying different heteroatoms such as nitrogen, boron, sulfur, or phosphorus, which broadens the heteroatom-doping scope.[25] Third, PILs are surface-active materials and are able to coat different surfaces (carbon, metal, or metal oxide).[26] Consequently, PIL-derived porous carbons can be flexibly designed in different morphologies such as spheres, nanotubes, and membranes, by templating or template-free methods.[27]

Recently, we prepared NPC composites with a nanostructured porosity via pyrolysis of polypyrrole deposited on the surface of graphene oxide (GO) nanosheet-stabilized PMMA particles that relied on the stabilizing power of GO nanosheets.[28–30] The resulting NPCs exhibited a specific surface area of 289–398 $m^2\ g^{-1}$ and a reversible capacity of 831 mA h g^{-1} at a current rate of 74.4 mA g^{-1} in LIBs. However, this reversible capacity decayed dramatically to 343 mA h g^{-1} at a higher rate of 744 mA g^{-1}.[28]

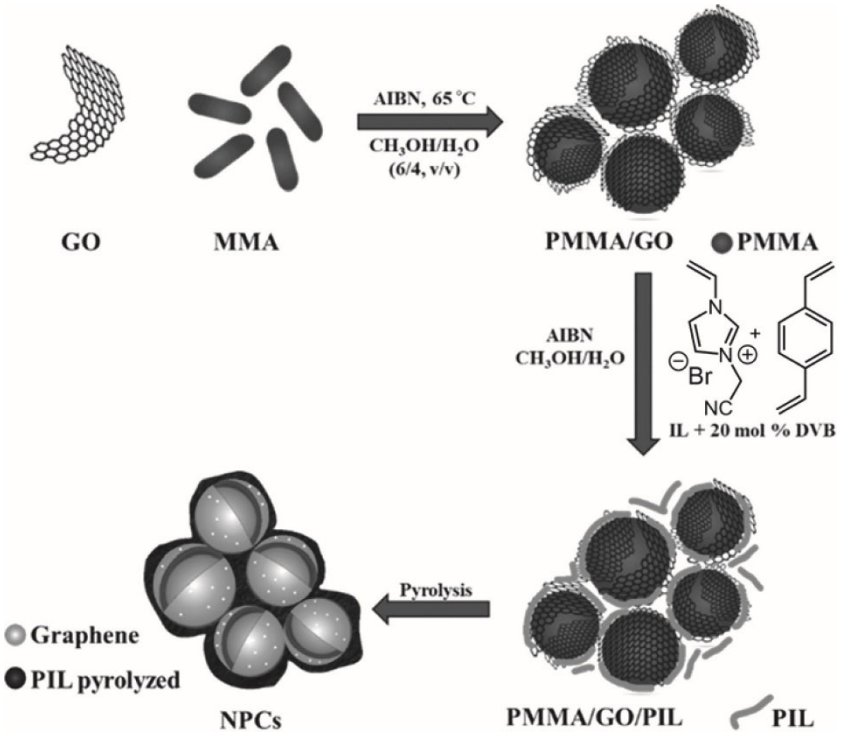

Scheme 1. Schematic illustration of the synthetic route toward NPCs from PIL, GO, and PMMA nanoparticles.

Published in : Macromolecular Rapid Communications (2019), vol. 40, issue 1, pp. 1-6
doi.org/10.1002/marc.201800545
Status : Postprint (Author's version)

In this contribution, poly(3cyanomethyl-1-vinylimidazolium bromide) PIL as a popular carbon precursor[13] was tested as NPC precursor in place of polypyrrole, which led to a NPC electrode of much better performance in LIBs and was further investigated as an SIB anode. As presented in **Scheme 1**, NPCs were synthesized by a templating method inspired by our previous work.[31] Briefly, a PMMA/GO hybrid template was prepared via dispersion polymerization of methyl methacrylate (MMA) in a water–methanol mixture in the presence of dispersed GO as stabilizer and 2,2'-azoisobutyronitrile (AIBN) as radical initiator.[30] During the polymerization, a phase separation occurred to form spherical particles of PMMA/GO with a particle size of 200–250 nm (Figure S2, Supporting Information). The PMMA/GO template was then decorated by a thin layer of PIL as precursor for N-doped carbon. 3-Cyanomethyl-1-vinylimidazolium bromide (CMVImBr) was chosen as the ionic liquid (IL) monomer, as it is rich in nitrogen and is well soluble in the reaction mixture. The free-radical copolymerization of this IL monomer with divinylbenzene (DVB) used as cross-linker ([CMVImBr]/ [DVB] = 4/1 in molar ratio) in the presence of the PMMA/GO particles in the medium leads to the formation of a PIL thin film around each particle. Scanning electron microscopy (SEM) analysis of the dried sample (**Figure 1**a) shows well-defined spherical particles of 250–300 nm in diameter. The strong interaction between the selected PIL and GO through non-covalent cation–π interactions as well as electrostatic attraction favors a homogeneous thin coating of PIL onto the surface of the preformed PMMA/GO particles.[32] The composition of these particles was investigated by Fourier transform infrared (ATR-FTIR) spectroscopy. Figure 1b compares the FTIR spectra of PMMA/GO and PMMA/GO/PCMVImBr. The characteristic peaks of PMMA/GO (C–O at 1147 cm^{-1}, C–O–C at 1435 cm^{-1}, and C=O at 1727 cm^{-1}, black line)[33,34] are all observed in that of PMMA/GO/PCMVImBr (red line). Compared to the PMMA/GO spectrum, new bands at 1170 and 1553 cm^{-1} in the PMMA/ GO/PCMVImBr sample are observed and associated to the C–N stretching of imidazolium rings and ring in-plane asymmetric stretching, CH_2(N) as well as CH_3(N)CN stretching vibrations of the PIL side chains, respectively.[35,36] The FTIR analysis confirms that PIL was successfully grown onto PMMA/GO particles in accordance with the SEM images.

The thermostability of the as-obtained PMMA/GO/PCMVImBr hybrid, that is, the NPC precursor, was checked by thermogravimetric analysis (TGA) under N_2 atmosphere and compared to the PMMA/GO template (Figure S3, Supporting Information). The major mass loss of PMMA/GO sample (black line) occurs between 200 and 400 °C, which is attributed to a decomposition of oxygen-containing groups in the GO and thermo-depolymerization of PMMA chains. A residue of 2.9 wt% was observed, which corresponds to carbon from the PMMA/GO sample. The PIL-containing NPC precursor (red line) has a much higher residue mass of 12.6 wt% at the same temperature.

Pyrolysis of PMMA/GO/PCMVImBr to generate NPCs was performed on a dry sample by a single-phase, stepwise thermal treatment. The first step was performed at 250 °C for 1 h under nitrogen to thermally depolymerize the sacrificial PMMA nanoparticle template, leaving behind macropores, and in parallel a thermal reduction of GO into graphene (rGO) nanosheets.[37] The second step involves pyrolysis of the PCMVImBr PIL network by heating at a rate of 5 °C min^{-1} until the desired temperature and then maintaining this temperature for 1 h. Two different final temperatures were used, that is, 800 and 900 °C,[38] yielding samples of NPC1 and NPC2, respectively. The morphology of the obtained NPCs was investigated by SEM (Figure 1c,d). Particle-like macroporous carbon products are clearly observed in both samples.

The crystalline phase of NPCs was studied by X-ray diffraction (XRD) measurement. Figure S4, Supporting Information, shows the XRD patterns of the two (NPC1 and NPC2) samples. NPC1 (blue curve) exhibits two main diffraction peaks at 2θ = 25.7° and 43.1,[39,40] which can be assigned, respectively, to the (002) and

Published in : Macromolecular Rapid Communications (2019), vol. 40, issue 1, pp. 1-6
doi.org/10.1002/marc.201800545
Status : Postprint (Author's version)

(100) planes of graphitic carbon. At a higher pyrolysis temperature to produce NPC2 (red curve), these two peaks appear at higher 2θ angles, indicating the formation of graphitic carbons of a higher order in atomic structure.[41] The mass percentage of nitrogen in NPCs samples was determined by elemental analysis (**Table 1**) to be 2.9 and 2.6 wt%, respectively, which is normal for PILs carrying Br^- as counter anion.[13,38]

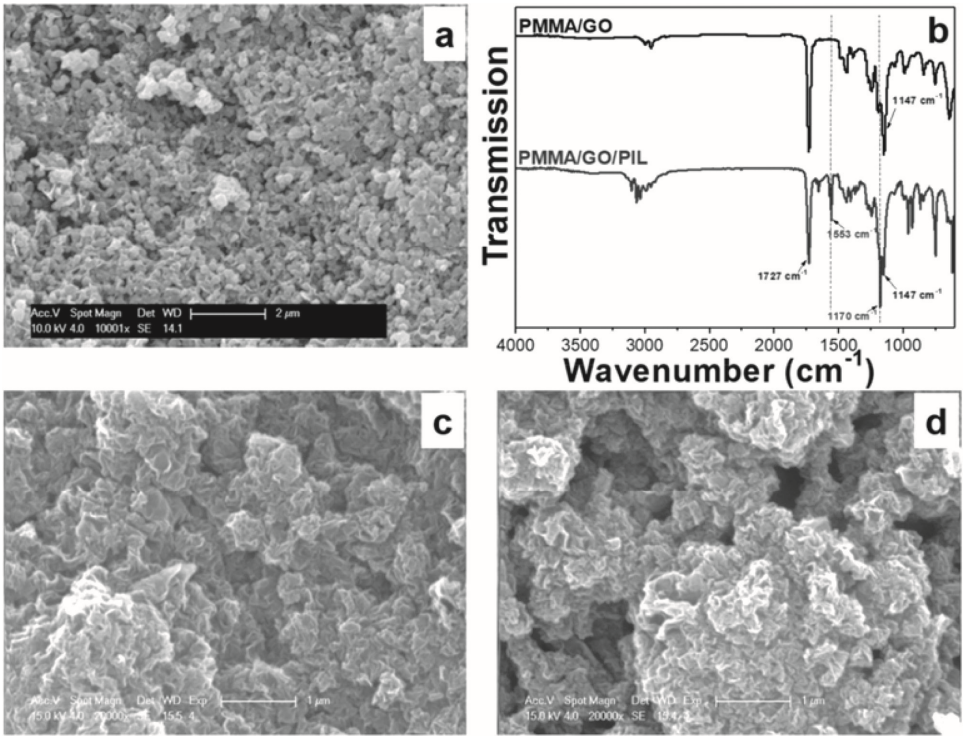

Figure 1. SEM images of a) PMMA/GO/PIL, c) NPC1, and d) NPC2. b) ATR-FTIR spectra of PMMA/GO and PMMA/GO/PIL.

The porous structure of NPCs was characterized by nitrogen sorption measurement at 77 K (**Figure 2**a,b). The Brunauer– Emmett–Teller specific surface area (S_{BET}) and the total pore volume are reported in Table 1. The hysteresis loops in the relative pressure of P/P_0 > 0.45 in the N_2 isotherms (Figure 2a) confirm the presence of mesopores, while the non-closure nature of the isotherm curve before P/P_0 – 1.0 implies the coexistence of macropores that are generated during the degradation of PMMA nanoparticle template.[42,43] In addition, the S_{BET} increases when NPCs are pyrolyzed at a higher temperature, that is, 424 $m^2\ g^{-1}$ at 800 °C and 561 $m^2 g^{-1}$ at 900 °C. The increase in S_{BET} might result from a higher extent of pyrolysis.[44] This presumption is supported by XRD measurement which indicates a better ordered graphitic structure at 900 °C than that at 800 °C. The pore size distribution curve of NPC1 and NPC2 samples

Table 1. Characteristics of NPC1 and NPC2 obtained at 800 and 900 °C, respectively.

Sample	Temperature of pyrolysis [°C]	N [wt%]	S_{BET} [$m^2\ g^{-1}$]	$V\mu$ [$cm^3\ g^{-1}$]
NPC1	800	2.9	424	1.07
NPC2	900	2.6	561	1.60

was obtained by the non-local density functional theory (NLDFT) method (Figure 2b). A broad-size distribution of mesopores is observed for both samples. One distinctive difference between these two samples is that the small fraction of micropores observed in NPC1 is completely absent in NPC2, that is, a full degradation of micropores at a higher pyrolysis temperature at the expense of growth of meso- and

Published in : Macromolecular Rapid Communications (2019), vol. 40, issue 1, pp. 1-6
doi.org/10.1002/marc.201800545
Status : Postprint (Author's version)

macropores.[44] This observation indicates that the micropores developed during the pyrolysis of PCMVImBr at 800 °C collapse and fuse into larger pores at 900 °C. The meso- and macropores observed for NPC1 and NPC2 originate from PMMA nanoparticle template degradation and the PIL precursor. It should be noted that the pyrolysis of PCMVImBr alone failed to produce porous carbon structure.[13] Because a wide-size distribution of mesopores/macropores in a hierarchical manner is expected to be beneficial to metal-ion batteries, the NPC samples were integrated in a half-cell for electrochemical tests.

Several electrochemical properties of NPCs were first investigated by cyclic voltammetry (CV) in a half-cell configuration at a scanning rate of 0.1 mV s^{-1} between 0 and 3.0 V (vs Li^+/Li). As shown in **Figure 3**a,b, both NPC electrodes present typical CV curves of porous carbon materials.[40,45] The large shoulder peak between 1 and 0.4 V in the first cathodic scan, which disappears in the other cathodic scans, can be attributed to side reactions on the electrode surface and interface due to formation of solid-electrolyte interphase (SEI) layer.[46] No apparent peak was recorded in anodic scan, indicating that lithium ion extraction from NPC has no specific voltage. It is important to note that the CV curves after the first scan almost overlapped with each other, indicating a stable reversibility in both NPC1 and NPC2 electrodes.

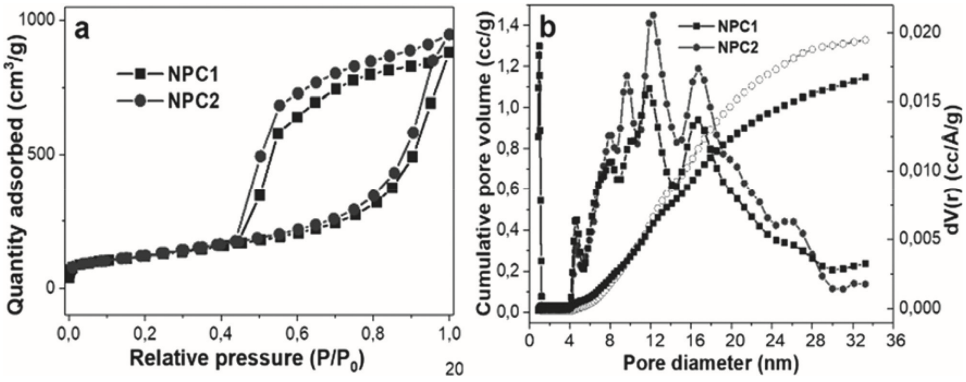

Figure 2. a) Nitrogen adsorption–desorption isotherms and b) pore-size distribution plots of NPC1 and NPC2.

Figure 3c,d present galvanostatic charge–discharge profiles of the first three cycles and the 200th cycle for the NPC1 and NPC2 electrodes/Li half-cell at a current density of 0.4 A g^{-1} between 0 and 3.0 V. The first cycle reveals a high discharge capacity of 1557 and 2251 mA h g^{-1} and a charge capacity of 916 and 981 mA h g^{-1} for NPC1 and NPC2, respectively, representing initial Coulombic efficiencies of 58.8% for NPC1 and 43.6% for NPC2. This irreversible capacity can be mainly ascribed to consumption of Li^+ in the formation of the SEI layer at the electrode–electrolyte interface and/or irreversible lithium ion insertion into highly active sites such as defects and in the vicinity of residual hydrogen atoms.[45,47,48] However, the irreversible capacity is reduced in the second cycle and the reversible capacity reaches 764 mA h g^{-1} for NPC1 and 1013 mAh g^{-1} for NPC2 after 200 cycles (3e). The Coulombic efficiency of both samples increases dramatically upon cycling, and reaches 99.1% for NPC1 and 98.2% for NPC2 after five cycles, indicating an improved reversibility of the Li^+ ion intercalation and deintercalation stability. Figure 3f presents the rate capability performances of NPC1 and NPC2 electrodes at various current densities from 0.4 to 4 A g^{-1}. As depicted in Figure 3f, the rate performance of the NPC2 is superior to NPC1. The NPC2 electrode delivers reversible charge/discharge capacities of 1046, 942, 790, 478, and 423 mA h g^{-1}, at current rates of 0.4, 0.8, 2, and 4 A g^{-1}, respectively. Then the reversible charge/discharge capacity is recovered to 1039 mA h g^{-1} when the current density is set back to 0.4 A g^{-1}, indicating an excellent rate capability of NPC2. In comparison to NPC1 or to the reported N-doped carbon derived from polypyrrole prepared in the same manner, NPC2

Published in : Macromolecular Rapid Communications (2019), vol. 40, issue 1, pp. 1-6
doi.org/10.1002/marc.201800545
Status : Postprint (Author's version)

exhibits excellent reversible capacity, high rate performances, and prolonged cycling stability.[28] The improved performance can be related to a higher specific surface area (561 $m^2 g^{-1}$) and hierarchically meso- and macroporous structure, offering a sufficient electrode–electrolyte interface to exchange Li ions.[49,50] Moreover, the inherent N dopant (2.6 and 2.2 wt% as shown in Table 1) in the carbon matrix is beneficial for enhanced reactivity and creates more Li^+ storage sites.[51] Table S1, Supporting Information, reports a

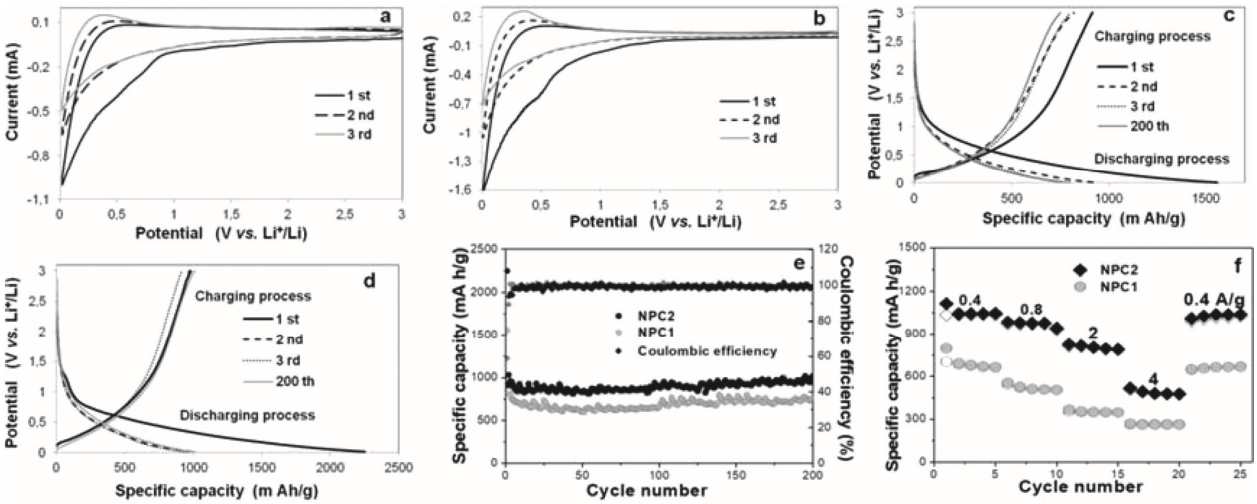

Figure 3. Cyclic voltammetry curves at a scan rate of 0.1 mV s^{-1} of a) NPC1 and b) NPC2 electrodes. Charge–discharge curves measured at 0.4 A g^{-1} of c) NPC1 and d) NPC2 electrodes. e) Cycle performance of the cells at a current rate of 0.4 A g^{-1} between 3.0 and 0 V versus Li^+/Li: specific capacity (circles) and Coulombic efficiency (diamonds) of the NPC1 (pink) and NPC2 (green) electrodes. f) Rate capabilities and cycle performance of the NPC1 (circles) and NPC2 (diamonds) electrodes at current densities from 0.4 to 4 A g^{-1}: discharge capacities (colored marks) and charge capacities (hollow marks).

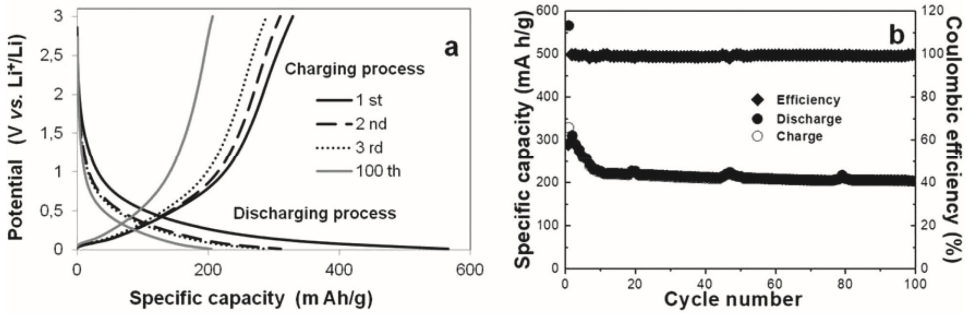

Figure 4. a) Charge–discharge curves and b) cycling performance: specific capacity (circles) and Coulombic efficiency (diamonds) of NPC2 electrode at a current density of 0.1 A g^{-1} between 0 and 3 V versus Na^+/Na.

comparison between the lithium storage performances of NPC2 and other N-doped carbons reported previously. It clearly shows that NCP2 delivers comparable or higher electrochemical performance than the best reported N-doped carbons in the literature.[52–54] This work shows that the nature of the polymer precursor for NPC and the pyrolysis temperature affect the structure characteristics of NPCs, such as specific surface area, the structured porosity, and N-doping level, and are effective ways to improve cycling performance of electrode for LIBs.[18,40,52,55–64]

The NPC2 electrode was further investigated as an anode for sodium storage in a half-cell conformation with sodium metal counter electrode and NaTFSI as electrolyte. **Figure 4**a displays charge/discharge profiles of NPC2 electrode in 1st, 2nd, 3rd, and 100th cycles between 0 and 3.0 V (vs Na^+/Na) at 0.1 A g^{-1}. The specific discharge capacity in the first cycle is 566 mA h g^{-1}, while the specific charge capacity is 329 mA h g^{-1},

Published in : Macromolecular Rapid Communications (2019), vol. 40, issue 1, pp. 1-6
doi.org/10.1002/marc.201800545
Status : Postprint (Author's version)

defining a Coulombic efficiency of 58%. This large irreversible capacity is mainly attributed to formation of a SEI layer, similar to the LIBs. The Na cell cycling performance in a potential window of 0–3.0 V at a current rate of 0.1 A g^{-1} is presented in 4b. After the initial cycle, the Coulombic efficiency increases to 99.8%. The reversible discharge capacities of NPC2 electrode after 100 cycles are maintained at 205 mA h g^{-1}, demonstrating good electrochemical performance of NPC2 electrode for SIBs. Similar to the LIBs, the high specific surface area and the hierarchically porous structure of NPC2 make an active surface accessible to the electrolyte and shortens the diffusion path for Na ions.[65–68] The capacities of SIBs are lower than LIBs due to the much bigger atomic radius of sodium ion (Na^+ 1.02 Å vs Li^+ 0.59 Å),[69] which leads to smaller discharge capacities due to poorer kinetics in SIBs compared to those in LIBs. The electrochemical performance of our NPC2 electrode is nevertheless satisfactory among candidates of anodes in SIBs reported recently.[70,71]

In summary, NPCs were successfully prepared using PIL as carbon precursor and PMMA nanoparticles stabilized by GO as sacrificial template. PIL provides the nitrogen source of NPCs and facilitates the formation of hierarchical pores. The correlation between pyrolysis temperature and the nature of NPCs was preliminarily investigated in terms of specific surface area and porosity. NPC2 obtained at 900 °C shows a larger specific surface area of 561 m^2 g^{-1} with hierarchical meso- and macropore structure and a nitrogen content of 2.6 wt%. More importantly, the NPC2 electrode displays a high reversible charge/discharge capacity of 1013 mA h g^{-1} after 200 cycles at 0.4 A g^{-1} for LIBs, and 205 mA h g^{-1} after 100 cycles at 0.1 A g^{-1} for SIBs. This good electrochemical performance clearly demonstrates that such NPCs are promising anode materials for both LIBs and SIBs. It is believed that without any complex techniques or post-treatments, this inexpensive strategy opens up a new stimulating platform for developing novel nitrogen-doped porous carbons from PIL for applications in energy storage, catalysis, and environmental treatment.

Experimental Section

The experimental details have been placed in the Supporting Information.

Acknowledgements

The authors thank the ITN Marie-Curie "Renaissance" funded by the People FP7 Programme, the "Fonds de la Recherche Scientifique" (FRS-FNRS), and the Belgian Science Policy in the frame of the Interuniversity Attraction Poles Program (P7/05)-Functional Supramolecular Systems (FS2) for financial supports. C.D. is research director of the FRS-FNRS. J.Y. thanks the Wallenberg Academy Fellow program of the Knut and Alice Wallenberg Foundation.

Conflict of Interest

The authors declare no conflict of interest.

Published in : Macromolecular Rapid Communications (2019), vol. 40, issue 1, pp. 1-6
doi.org/10.1002/marc.201800545
Status : Postprint (Author's version)

[1] Y. Zhang, X. Zhang, X. Ma, W. Guo, C. Wang, T. Asefa, X. He, *Sci. Rep.* **2017**, *7*, 43366.
[2] S. Zhong, Q. Wang, D. Cao, *Sci. Rep.* **2016**, *6*, 21295.
[3] J. Gong, H. Lin, M. Antonietti, J. Yuan, *J. Mater. Chem. A* **2016**, *4*, 7313.
[4] Z. Jiang, Z.-J. Jiang, X. Tian, L. Luo, *Electrochim. Acta* **2014**, *146*, 455.
[5] L. Bi, S. Ci, P. Cai, H. Li, Z. Wen, *Appl. Surf. Sci.* **2018**, *427*, 10.
[6] B. Qiu, C. Pan, W. Qian, Y. Peng, L. Qiu, F. Yan, *J. Mater. Chem. A* **2013**, *1*, 6373.
[7] X. Zhang, G. Zhu, M. Wang, J. Li, T. Lu, L. Pan, *Carbon* **2017**, *116*, 686.
[8] D. Li, L. Zhang, H. Chen, J. Wang, L.-X. Ding, S. Wang, P. J. Ashman, H. Wang, *J. Mater. Chem. A* **2016**, *4*, 8630.
[9] Z.-S. Wu, W. Ren, L. Xu, F. Li, H.-M. Cheng, *ACS Nano* **2011**, *5*, 5463.
[10] H. Liu, M. Jia, B. Cao, R. Chen, X. Lv, R. Tang, F. Wu, B. Xu, *J. Power Sources* **2016**, *319*, 195.
[11] H. Wang, C. Yuan, R. Zhou, Q. Duan, Y. Li, *Chem. Eng. J.* **2017**, *316*, 1004.
[12] S.-W. Park, J.-C. Kim, M. A. Dar, H.-W. Shim, D.-W. Kim, *Chem. Eng. J.* **2017**, *315*, 1.
[13] Q. Zhao, T.-P. Fellinger, M. Antonietti, J. Yuan, *J. Mater. Chem. A* **2013**, *1*, 5113.
[14] B. Xu, D. Zheng, M. Jia, G. Cao, Y. Yang, *Electrochim. Acta* **2013**, *98*, 176.
[15] D. Yu, L. Zhou, J. Tang, J. Li, J. Hu, C. Peng, H. Liu, *Ind. Eng. Chem. Res.* **2017**, *56*, 8880.
[16] X. Zhou, P. Wang, Y. Zhang, L. Wang, L. Zhang, L. Zhang, L. Xu, L. Liu, *J. Mater. Chem. A* **2017**, *5*, 12958.
[17] S. Tanaka, N. Nishiyama, Y. Egashira, K. Ueyama, *Chem. Commun.* **2005**, *0*, 2125.
[18] D. Li, L.-X. Ding, H. Chen, S. Wang, Z. Li, M. Zhu, H. Wang, *J. Mater. Chem. A* **2014**, *2*, 16617.
[19] C. H. Kim, D.-K. Lee, T. J. Pinnavaia, *Langmuir* **2004**, *20*, 5157.
[20] N. P. Wickramaratne, J. Xu, M. Wang, L. Zhu, L. Dai, M. Jaroniec, *Chem. Mater.* **2014**, *26*, 2820.
[21] J. P. Paraknowitsch, A. Thomas, J. Schmidt, *Chem. Commun.* **2011**, *47*, 8283.
[22] S. Yang, R. E. Bachman, X. Feng, K. Müllen, *Acc. Chem. Res.* **2013**, *46*, 116.
[23] J. Yuan, C. Giordano, M. Antonietti, *Chem. Mater.* **2010**, *22*, 5003.
[24] W. Qian, J. Texter, F. Yan, *Chem. Soc. Rev.* **2017**, *46*, 1124.
[25] Y. Men, M. Ambrogi, B. Han, J. Yuan, *Int. J. Mol. Sci.* **2016**, *17*, 532.
[26] J. Yuan, M. Antonietti, *Polymer* **2011**, *52*, 1469.
[27] S. Soll, T.-P. Fellinger, X. Wang, Q. Zhao, M. Antonietti, J. Yuan, *Small* **2013**, *9*, 4135.
[28] W. Alkarmo, F. Ouhib, A. Aqil, J.-M. Thomassin, B. Vertruyen, M.-L. Piedboeuf, N. Job, C. Detrembleur, C. Jérôme, *J. Mater. Sci.* **2018**, *53*, 6135.
[29] J. Texter, *Curr. Opin. Colloid Interface Sci.* **2015**, *20*, 454.
[30] J. M. Thomassin, M. Trifkovic, W. Alkarmo, C. Detrembleur, C. Jerome, C. Macosko, *Macromolecules* **2014**, *47*, 2149.
[31] W. Alkarmo, A. Aqil, F. Ouhib, J.-M. Thomassin, D. Mazouzi, D. Guyomard, C. Detrembleur, C. Jerome, *New J. Chem.* **2017**, *41*, 10555.
[32] X. Zhou, T. Wu, K. Ding, B. Hu, M. Hou, B. Han, *ChemComm.* **2010**, *46*, 386.
[33] S. Heo, S. Y. Cho, D. H. Kim, Y. Choi, H. H. Park, H.-J. Jin, *J. Nanosci. Nanotech.* **2012**, *12*, 5990.
[34] P. K. Ghosh, A. Kumar, K. Kumar, *Polym. Sci. Ser. A* **2015**, *57*, 829.
[35] H. Song, H. Lin, M. Antonietti, J. Yuan, *Adv. Mater. Interfaces* **2016**, *3*, 1500743.
[36] K. Grygiel, B. Wicklein, Q. Zhao, M. Eder, T. Pettersson, L. Bergstrom, M. Antonietti, J. Yuan, *ChemComm.* **2014**, *50*, 12486. [37] S. Pei, H.-M. Cheng, *Carbon* **2012**, *50*, 3210.
[38] T.-P. Fellinger, A. Thomas, J. Yuan, M. Antonietti, *Adv. Mater.* **2013**, *25*, 5838.
[39] F. Xu, Y. Lai, R. Fu, D. Wu, *J. Mater. Chem. A* **2013**, *1*, 5001.
[40] L. Qie, W. Chen, Z. Wang, Q. Shao, X. Li, L. Yuan, X. Hu, W. Zhang, Y. Huang, *Adv. Mater.* **2012**, *24*, 2047.
[41] W. Niu, L. Li, X. Liu, N. Wang, J. Liu, W. Zhou, Z. Tang, S. Chen, *J. Am. Chem. Soc.* **2015**, *137*, 5555.
[42] P. K. Tripathi, M. Liu, Y. Zhao, X. Ma, L. Gan, O. Noonan, C. Yu, *J. Mater. Chem. A* **2014**, *2*, 8534.
[43] P. K. Tripathi, L. Gan, M. Liu, X. Ma, Y. Zhao, D. Zhu, Z. Xu, L. Chen, N. N. Rao, *Mater. Lett.* **2014**, *120*, 108.
[44] X. Liu, L. Zhou, Y. Zhao, L. Bian, X. Feng, Q. Pu, *ACS Appl. Mater. Interfaces* **2013**, *5*, 10280.
[45] F.-D. Han, Y.-J. Bai, R. Liu, B. Yao, Y.-X. Qi, N. Lun, J.-X. Zhang, *Adv. Energy Mater.* **2011**, *1*, 798.
[46] A. L. M. Reddy, A. Srivastava, S. R. Gowda, H. Gullapalli, M. Dubey, P. M. Ajayan, *ACS Nano* **2010**, *4*, 6337.
[47] G. Zhou, D.-W. Wang, X. Shan, N. Li, F. Li, H.-M. Cheng, *J. Mater. Chem.* **2012**, *22*, 11252.
[48] K. T. Lee, J. C. Lytle, N. S. Ergang, S. M. Oh, A. Stein, *Adv. Funct. Mater.* **2005**, *15*, 547.
[49] R. Song, H. Song, X. Chen, Y. Cui, J. Zhou, S. Zhang, *Electrochim. Acta* **2014**, *127*, 186.
[50] J. R. Dahn, T. Zheng, Y. Liu, J. S. Xue, *Science* **1995**, *270*, 590.

[51] X. Jia, G. Zhang, T. Wang, X. Zhu, F. Yang, Y. Li, Y. Lu, F. Wei, *J. Mater. Chem. A* **2015**, *3*, 15738.
[52] D. Nan, Z.-H. Huang, R. Lv, L. Yang, J.-G. Wang, W. Shen, Y. Lin, X. Yu, L. Ye, H. Sun, F. Kang, *J. Mater. Chem. A* **2014**, *2*, 19678.
[53] C. He, R. Wang, H. Fu, P. K. Shen, *J. Mater. Chem. A* **2013**, *1*, 14586.
[54] X. Liu, J. Zhang, S. Guo, N. Pinna, *J. Mater. Chem. A* **2016**, *4*, 1423.
[55] F. Zheng, Y. Yang, Q. Chen, *Nat. Commun.* **2014**, *5*, 5261.
[56] X. Zhou, J. Tang, J. Yang, J. Xie, B. Huang, *J. Mater. Chem. A* **2013**, *1*, 5037.
[57] S.-X. Wang, L. Yang, L. P. Stubbs, X. Li, C. He, *ACS Appl. Mater. Interfaces* **2013**, *5*, 12275.
[58] Z. Li, Z. Xu, X. Tan, H. Wang, C. M. B. Holt, T. Stephenson, B. C. Olsen, D. Mitlin, *Energy Environ. Sci.* **2013**, *6*, 871.
[59] Z.-Y. Sui, C. Wang, Q.-S. Yang, K. Shu, Y.-W. Liu, B.-H. Han, G. G. Wallace, *J. Mater. Chem. A* **2015**, *3*, 18229.
[60] Y. Liu, X. Wang, Y. Dong, Z. Wang, Z. Zhao, J. Qiu, *J. Mater. Chem. A* **2014**, *2*, 16832.
[61] L.-L. Tian, X.-Y. Wei, Q.-C. Zhuang, C.-H. Jiang, C. Wu, G.-Y. Ma, X. Zhao, Z.-M. Zong, S.-G. Sun, *Nanoscale* **2014**, *6*, 6075.
[62] X. Li, X. Zhu, Y. Zhu, Z. Yuan, L. Si, Y. Qian, *Carbon* **2014**, *69*, 515.
[63] G. Tan, W. Bao, Y. Yuan, Z. Liu, R. Shahbazian-Yassar, F. Wu, K. Amine, J. Wang, J. Lu, *J. Mater. Chem. A* **2017**, *5*, 5532.
[64] C. Liu, X. Liu, J. Tan, Q. Wang, H. Wen, C. Zhang, *J. Power Sources* **2017**, *342*, 157.
[65] D. Wang, X. Li, J. Yang, J. Wang, D. Geng, R. Li, M. Cai, T.-K. Sham, X. Sun, *Phys. Chem. Chem. Phys.* **2013**, *15*, 3535.
[66] J. Qin, C. He, N. Zhao, Z. Wang, C. Shi, E.-Z. Liu, J. Li, *ACS Nano* **2014**, *8*, 1728.
[67] J. Liu, P. Kopold, C. Wu, P. A. van Aken, J. Maier, Y. Yu, *Energy Environ. Sci.* **2015**, *8*, 3531.
[68] H. Z. Li, L. Y. Yang, J. Liu, S. T. Li, L. B. Fang, Y. K. Lu, H. R. Yang, S. L. Liu, M. Lei, *J. Power Sources* **2016**, *324*, 780.
[69] C. Zhu, X. Mu, P. A. van Aken, Y. Yu, J. Maier, *Angew. Chem. Int. Ed.* **2014**, *53*, 2152.
[70] J. Shen, W. Hu, Y. Li, L. Li, X.-J. Lv, L. Zhang, *J. Alloys Comp.* **2017**, *701*, 372.
[71] L.-L. Tian, S.-B. Li, M.-J. Zhang, S.-K. Li, L.-P. Lin, J.-X. Zheng, Q.-C. Zhuang, K. Amine, F. Pan, *ACS Appl. Mater. Interfaces* **2016**, *8*, 26722.